Conditional Detection of Pure Quantum States of Light after Storage in a Tm-Doped Waveguide

Erhan Saglamyurek,[1] Neil Sinclair,[1] Jeongwan Jin,[1] Joshua A. Slater,[1] Daniel Oblak,[1] Félix Bussières,[1,*] Mathew George,[2] Raimund Ricken,[2] Wolfgang Sohler,[2] and Wolfgang Tittel[1]

[1]*Institute for Quantum Information Science, and Department of Physics and Astronomy, University of Calgary, 2500 University Drive NW, Calgary, Alberta T2N 1N4, Canada*

[2]*Department of Physics—Applied Physics, University of Paderborn, Warburger Strasse 100, 33095 Paderborn, Germany*

(Received 3 November 2011; published 22 February 2012)

We demonstrate the conditional detection of time-bin qubits after storage in and retrieval from a photon-echo–based waveguide quantum memory. Each qubit is encoded into one member of a photon pair produced via spontaneous parametric down-conversion, and the conditioning is achieved by the detection of the other member of the pair. By performing projection measurements with the stored and retrieved photons onto different bases, we obtain an average storage fidelity of 0.885 ± 0.020, which exceeds the relevant classical bounds and shows the suitability of our integrated light-matter interface for future applications of quantum information processing.

DOI: 10.1103/PhysRevLett.108.083602 PACS numbers: 42.50.Ex, 03.67.Hk, 32.80.Qk, 78.47.jf

Quantum memories are key elements for future applications of quantum information science such as long-distance quantum communication via quantum repeaters [1,2] and, more generally, distributed quantum information processing in quantum networks [3]. They enable reversible mapping of arbitrary quantum states between traveling and stationary carriers (i.e., light and matter). This reduces the impact of loss on the time required to establish entanglement between distant locations [1] and allows the implementation of local quantum computers based on linear optics [4]. However, towards these ends, the successful transfer of a quantum state into the memory must be announced by a heralding signal. When using an individual absorber, such a signal can be derived through the detection of a change of atomic level population [5]. In atomic ensembles, this approach is infeasible. Instead, storage is derived from the detection of a second photon that indicates either the absorption [6] or the presence of the first at the input of the memory [7] (the first approach relies on spontaneous Raman scattering and the second on using pairs of photons). Furthermore, quantum memories must have large acceptance bandwidths and multimode capacities and allow on-demand readout after second-long storage with high efficiency [7,8]. In addition, for viable quantum technology, quantum memories should be robust and simple to operate (e.g., be based on integrated optics).

A lot of progress towards these figures of merit has been reported over the past few years, including work that explores electromagnetically induced transparency, as well as photon-echo and cavity QED-based approaches (see [2,5,7–16] for reviews and the latest achievements). For instance, quantum memories employing Rb vapor have demonstrated efficiencies up to 87% [9] and storage times in excess of 0.1 s [10], while gigahertz bandwidths [11] and storage of 64 modes [14] have been shown in rare-earth materials. However, having a quantum memory that simultaneously satisfies all figures of merit currently remains an outstanding challenge.

Yet, strictly, most of these experiments did not report true heralding—either heralding was not actually implemented, the ''heralding'' signal was generated only after the stored photon left the memory, or the signal could, due to technical issues, be derived only once the stored photon was detected. Nevertheless, experiments that employ photon pairs [11–13,17] do gain from conditioning the detection of the stored photon on that of the auxiliary photon (i.e., *a posteriori* heralding): By reducing the effects of loss and detector noise, conditioning generally increases the fidelity between the quantum state of the original and the retrieved photon.

Supplementing the experiments on storage of entangled photons [11–13,17], we now report another step towards the goal of building universal, viable, and heralded quantum memory devices—the storage of photons in pure quantum states in a solid-state waveguide, their retrieval, and their conditional detection by means of temporal correlations with auxiliary photons. We point out that the step to true heralding is minor and of a purely technical nature; it simply requires using different, existing, single-photon detectors (see, e.g., [18,19]).

Our experimental setup consists of two main blocks (see Fig. 1): a spontaneous parametric down-conversion (SPDC) photon-pair source and a $Ti:Tm:LiNbO_3$ single-mode waveguide fabricated by indiffusion processes [20]. When cooled to 3 K, and by using a photon-echo quantum memory protocol [7,8,21], the Tm-doped waveguide allows storage and retrieval of quantum states encoded into one member of each photon pair, while the detection of the other member provides the conditioning signal.

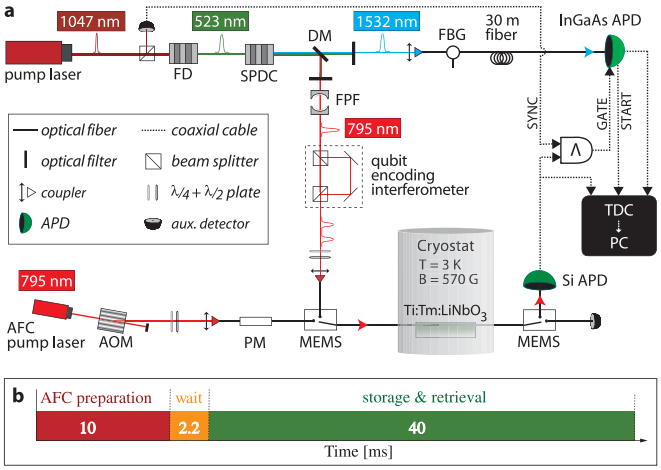

FIG. 1 (color online). (a) Photon-pair source and quantum memory setup (see the text for details). Wave plates align light polarization along the $LiNbO_3$'s C_3 axis. The waveguide is held at 3 K, and a 570 G magnetic field is applied along the crystal's C_3 axis [see Fig. 2(a)]. (b) Timing sequence containing three repeated phases: 10 ms AFC preparation for optical pumping, 2.2 ms *wait* to allow excited population to decay, and 40 ms *storage and retrieval*, during which 795 nm photons are successively stored for $t_{st} = 6$ ns and then recalled.

In the photon-pair source, a mode-locked pump laser generates 6 ps long pulses at a rate of 80 MHz and 1047.328 nm central wavelength. They are subsequently frequency-doubled (FD) in a periodically poled $LiNbO_3$ (PPLN) crystal, yielding pulses with 523.664 nm central wavelength, 16 ps duration, and 90 mW average power. The FD pulses are sent to a second PPLN crystal that, via SPDC, produces pairs of photons centered at 795.506 and 1532.426 nm. Frequency filtering the 795 nm photons with a 6 GHz-bandwidth Fabry-Pérot filter (FPF) and the 1532 nm photons with a 9 GHz-bandwidth fiber-Bragg grating (FBG), we obtain frequency uncorrelated pairs. Each 795 nm photon travels through an imbalanced, temperature-stabilized Mach-Zehnder interferometer with 42 cm path-length difference, corresponding to 1.4 ns relative delay. Thus, each photon emerges in a superposition of two temporal modes (early and late), i.e., in a time-bin qubit state [22]. They are then directed into the quantum memory, stored, retrieved, and finally detected by a Si avalanche-photodiode (APD)-based single-photon detector.

All 1532 nm photons are sent through 30 m standard telecommunication fiber to an InGaAs APD-based single-photon detector. As is typically done, the detector is gated to reduce noise. The gate signal could, in principle, be the SYNC signal [see Fig. 1(a)] derived from each pulse emitted by the pump laser. However, as its repetition rate of 80 MHz by far exceeds the maximum gate frequency of our detector, around 1 MHz, we first AND the SYNC pulses with pulses generated by each Si-APD detection and then use this low-rate signal to gate the InGaAs APD. Provided the latter is ready for photon detection (i.e., not deadtime-blocked due to a previous detection), this signal also starts a time-to-digital converter (TDC), which then records the time difference between the detection events produced by the Si APD and the InGaAs APD. These data are used to obtain statistics for single detections of the retrieved 795 nm photons, as well as for detections conditioned on the existence of 1532 nm photons. We emphasize that if an InGaAs APD supporting 80 MHz gate rate had been available [18,19], then 1532 nm photons could have been detected without the need for *a priori* detection of a 795 nm photon. This simple modification of our setup would have turned the conditional detection of 795 nm photons into detections that are heralded by clicks of the InGaAs APD.

The other main block of our setup is a Ti : Tm : $LiNbO_3$ waveguide that allows storage and retrieval of the 795 nm photons via the atomic frequency comb (AFC) quantum memory protocol [21]. This approach to quantum state storage requires the spectral absorption of an atomic ensemble to be constituted of a series of equally spaced lines with frequency spacing Δ_ν. The interaction between such an AFC and a photon with wave vector k leads to the absorption of the photon and generates a collective excitation in the atomic medium that is described by

$$|\Psi\rangle = \frac{1}{\sqrt{N!}} \sum_{j=1}^{N} c_j e^{i2\pi m_j \Delta_\nu t} e^{-ikz_j} |g_1, \ldots e_j, \ldots g_N\rangle. \quad (1)$$

Here, $|g_j\rangle$ ($|e_j\rangle$) denotes the ground (excited) state of atom j, $m_j\Delta_\nu$ is the detuning of the atom's transition frequency from the photon carrier frequency, z_j is its position measured along the propagation direction of the light, and the factor c_j depends on the atom's resonance frequency and position. Because of the presence of different atomic transition frequencies, the excited collective coherence dephases rapidly. However, the particular shape of the absorption line results in the recovery of the collective coherence after storage time t_{st}. This can easily be seen from Eq. (1): For $t = 1/\Delta_\nu$ all frequency-dependent phase factors are zero (mod 2π). This leads to reemission of the photon into the original mode and quantum state with maximally 54% efficiency for an optimally implemented AFC. Modifications to the procedure enable recall on demand and up to 100% efficiency [21].

Suitable media in which to implement the AFC protocol are cryogenically cooled rare-earth ion doped crystals [7,23]. They feature inhomogeneously broadened absorption profiles, often possess long-lived atomic sublevels that can serve as shelving levels for tailoring the AFC through persistent spectral hole burning, and generally have long coherence times on optical and spin transitions. We use the $^3H_6$–$^3H_4$ transition of Tm ions in a single-mode channel waveguide fabricated by Ti indiffusion into the Tm-doped

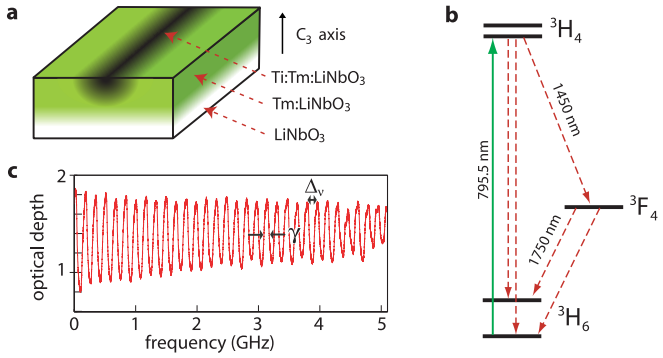

FIG. 2 (color online). (a) Waveguide geometry: The sample surface is first doped by indiffusing a ≈ 20 nm-thick Tm layer yielding a concentration profile of ≈ 6 μm depth with $\approx 10^{20}$ ions per cm^3 surface concentration. Subsequently, a 3 μm-wide channel waveguide is fabricated by indiffusion of a 40 nm-thick vacuum-deposited Ti stripe. AFC preparation light and single photons are coupled in and out of the waveguide with 10% total efficiency by butt-coupling single-mode fibers. (b) Simplified energy level diagram of Tm ions: The optical coherence time of the $^3H_6$–$^3H_4$ transition at 3 K is 1.6 μs, and the radiative lifetimes of the $^3H_4$ and $^3F_4$ levels are 82 μs and 2.4 ms, respectively. A 570 G magnetic field splits the ground and excited levels into Zeeman sublevels. The ground Zeeman level splitting is ~83 MHz, and the lifetime of the upper ground level exceeds 1 s. (c) 5 GHz-bandwidth AFC: The tooth separation is $\Delta_\nu = 167$ MHz, corresponding to 6 ns storage time. The linewidth of the teeth is $\gamma = 83$ MHz.

surface of a Z-cut $LiNbO_3$ crystal; see Fig. 2(a) [20]. To tailor the desired AFC into the inhomogeneously broadened absorption profile, Tm ions with transition frequencies within the comb's troughs are optically pumped via the excited level into long-lived nuclear Zeeman levels; see Fig. 2(b) [20,24]. To achieve frequency selective optical pumping, we employed a linear sideband chirp technique [11,25] that allowed us to create a 5 GHz broad grating (matching the spectral width of the 795 nm photons) with a tooth spacing of 167 MHz; see Fig. 2(c). This corresponds to a storage time of 6 ns. After each 10 ms-long AFC preparation, a 2.2 ms-long wait time allows atoms excited by the optical pumping to decay before photon storage [see Fig. 1(b) for the timing per experimental cycle]. A set of microelectromechanical switches (MEMS) then open the channel for qubits to enter the memory and, after recall, direct them towards the Si APD. We assessed our memory's retrieval efficiency to be $(2 \pm 0.5)\%$. By taking the 10 dB fiber-to-fiber coupling loss in and out of the waveguide into account, this yields an overall system efficiency of approximately 0.2% [11].

An interesting and useful aspect of photon-echo quantum memory protocols is that they provide a robust tool to manipulate time-bin qubits [26–29]. For example, by using the AFC approach, any projection measurement on time-bin qubit states can be performed by superimposing two

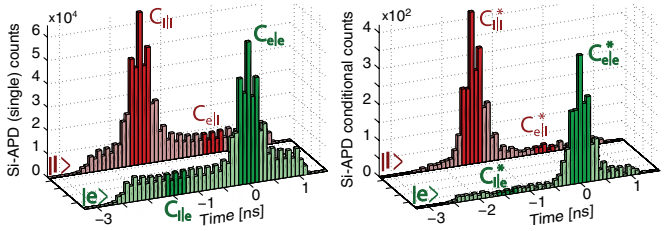

FIG. 3 (color online). Storage of early and late time-bin qubit states in the AFC memory. The left-hand figure depicts the histograms from 180 min of single detections of the retrieved 795 nm photons prepared in early (red) and late (green) qubit states with the highlighted regions marking the relevant detection windows. The right-hand figure shows the detections conditioned on 1532 nm photons for the same states. Without conditioning, the fidelities are $\mathcal{F}_e = 0.8652 \pm 0.0006$ and $\mathcal{F}_l = 0.8376 \pm 0.0004$ for the storage of early and late time-bin states, respectively. Correspondingly, with conditioning, the fidelities are $\mathcal{F}_e^* = 0.9505 \pm 0.0058$ and $\mathcal{F}_l^* = 0.9573 \pm 0.0033$.

combs (double AFC) with appropriately chosen relative center frequencies and amplitudes [27]. This leads to two reemission times that can be set to differ by the temporal mode separation of the qubit to be analyzed (1.4 ns for our experiments). Hence, as a previously absorbed photon is reemitted by the superimposed combs, early and late temporal modes interfere, allowing the qubit state to be analyzed in the same way as is typically done with an imbalanced Mach-Zehnder interferometer [27]. Double AFC recall will, however, lead to a reduction of the recall efficiency (compared to single recall).

To demonstrate faithful storage and retrieval of quantum states from the memory, we performed projection measurements with various time-bin qubits onto different bases using single (standard) and double AFC schemes as explained before. In all our measurements, the average photon number per qubit was 0.1 at the output of the qubit-encoding interferometer. First we generated qubit states that occupy only early $|e\rangle$ or late $|l\rangle$ temporal modes by blocking either the long or short arm of the qubit-encoding interferometer, respectively, and then stored these states in the memory for 6 ns. Figure 3 (left) shows single detections (no conditioning) of the retrieved photons as a function of the time difference with respect to the START signal. The dark counts from the Si APD reduce the signal to noise ratio (SNR) to ~5. For an input state $|e\rangle$, we compute the fidelity as $\mathcal{F}_e = C_{e|e}/(C_{e|e} + C_{l|e})$, where, e.g., $C_{l|e}$ denotes the number of detected counts in the late time bin given that $|e\rangle$ was encoded in the qubit at the input. Similarly, we can find $\mathcal{F}_l$, enabling us to calculate the mean fidelity: $\mathcal{F}_{el} = (\mathcal{F}_e + \mathcal{F}_l)/2 = 0.8514 \pm 0.0004$.

On the other hand, conditioning the detections of the retrieved photons on the detection of 1532 nm photons leads to a substantial increase of the SNR to ~22, as shown in Fig. 3 (right). This yields a mean fidelity of $\mathcal{F}_{el}^* = 0.9539 \pm 0.0024$.

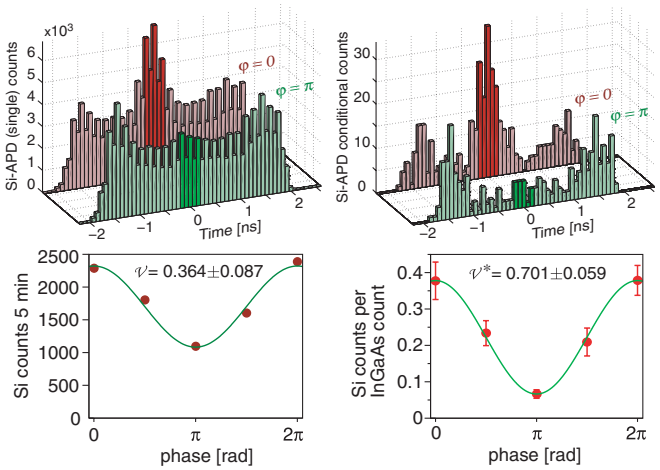

FIG. 4 (color online). Retrieval of qubits created in a superposition of early and late temporal modes. The top left figure presents histograms of single detections of the retrieved 795 nm photons with AFC phase settings of zero (red) and π (green), collected during 80 min. The top right figure shows the same histograms for conditional detections. The highlighted regions mark detection windows used to derive projection probabilities required to calculate fidelities. The lower curves show single and coincidence counts obtained for all phase settings for single detections (left) and conditional detections (right), yielding visibilities of 0.364 ± 0.087 and 0.701 ± 0.059, respectively.

Next, qubit states in an equal superposition of early and late temporal modes $(1/\sqrt{2})(|e\rangle + e^{i\phi}|l\rangle)$ were produced with ϕ set to zero. Storage and projection measurements were performed by using the double AFC scheme with the relative phase of the two combs (measured with respect to the phase introduced by the qubit-encoding interferometer) varied by $\pi/2$ increments. The results for single and conditional detections are given in Fig. 4. The histograms show the detection statistics for zero and π double AFC phase settings, from which we extract a SNR slightly above 1 for the single and above 6 for the conditional detection. In the lower part of Fig. 4, we show the normalized counts for each projection setting for the single and conditional detections. Fitting sinusoidal curves to these, we derive visibilities $\mathcal{V}$, which, in turn, yield a fidelity $\mathcal{F} = (1 + \mathcal{V})/2$ for single detections of $\mathcal{F}_\phi = 0.682 \pm 0.020$. For conditional detections, we find a significantly larger value of $\mathcal{F}^*_\phi = 0.851 \pm 0.030$. These figures allow establishing an average, single detection fidelity: $\overline{\mathcal{F}} \equiv (\mathcal{F}_{el} + 2\mathcal{F}_\phi)/3 = 0.738 \pm 0.029$. This violates the quantum-classical bound [30] of $\sim$0.667, thus verifying that our memory outperforms any classical storage protocol. However, it is below the bound of $\sim$0.833 for an optimal universal quantum cloner [31]. Harnessing the conditional detection, we find $\overline{\mathcal{F}^*} = 0.885 \pm 0.020$. This beats the quantum-classical bound by 10 standard deviations and also violates the optimal universal quantum cloner bound by 2.5 standard deviations.

In conclusion, we have demonstrated storage, retrieval, and conditional detection of different time-bin qubit states using a solid-state Ti : Tm : $LiNbO_3$ waveguide quantum memory with average fidelity $\overline{\mathcal{F}^*} = 0.885 \pm 0.020$, which exceeds the relevant classical bounds. Operating the memory in a heralded fashion is readily achievable with high-rate APDs that have recently become commercially available. Despite our memory device's current limitations, namely, efficiency, storage time, and preset recall time, the high fidelity and the wide spectral acceptance make our approach promising for future quantum communication schemes and quantum networks. The $LiNbO_3$ host crystal and the waveguide structure have potential advantages in quantum memory applications such as fast electric field control of collective atomic phase evolution, and, due to the resemblance with building blocks of classical integrated optical devices [32], it holds promise for simple integration with existing information technology. Furthermore, the ability to perform projection measurements using a photon-echo memory provides a simple and robust tool that might find use in other applications of quantum information processing.

We thank C. La Mela and T. Chanelière for helping in the initial stages of this work, V. Kiselyov for technical support, and NSERC, GDC, iCORE (now part of AITF), QuantumWorks, CFI, and AET for financial support. D. O. thanks the Carlsberg Foundation, and F. B. thanks FQRNT for support.

*Present address: Group of Applied Physics, University of Geneva, Chemin de Pinchat 22, 1211 Geneva, Switzerland.

[1] H.-J. Briegel *et al.*, Phys. Rev. Lett. **81**, 5932 (1998).
[2] N. Sangouard *et al.*, Rev. Mod. Phys. **83**, 33 (2011).
[3] J. Kimble, Nature (London) **453**, 1023 (2008).
[4] P. Kok *et al.*, Rev. Mod. Phys. **79**, 135 (2007).
[5] H. P. Specht *et al.*, Nature (London) **473**, 190 (2011).
[6] H. Tanji *et al.*, Phys. Rev. Lett. **103**, 043601 (2009).
[7] W. Tittel *et al.*, Laser Photon. Rev. **4**, 244 (2010).
[8] A. I. Lvovsky, B. C. Sanders and W. Tittel, Nature Photon. **3**, 706 (2009).
[9] M. Hosseini *et al.*, Nature Phys. **7**, 794 (2011).
[10] A. G. Radnaev *et al.*, Nature Phys. **6**, 894 (2010).
[11] E. Saglamyurek *et al.*, Nature (London) **469**, 512 (2011).
[12] C. Clausen *et al.*, Nature (London) **469**, 508 (2011).
[13] H. Zhang *et al.*, Nature Photon. **5**, 628 (2011).
[14] I. Usmani *et al.*, Nature Commun. **1**, 12 (2010).
[15] K. F. Reim *et al.*, Phys. Rev. Lett. **107**, 053603 (2011).
[16] M. Hedges *et al.*, Nature (London) **465**, 1052 (2010).
[17] K. Akiba *et al.*, New J. Phys. **11**, 013049 (2009).
[18] M. D. Eisaman *et al.*, Rev. Sci. Instrum. **82**, 071101 (2011).
[19] ID Quantique SA, Phys. Today **64**, 59 (2011).
[20] N. Sinclair *et al.*, J. Lumin. **130**, 1586 (2010).
[21] M. Afzelius *et al.*, Phys. Rev. A **79**, 052329 (2009).

[22] W. Tittel and G. Weihs, Quantum Inf. Comput. **1**, No. 2, 3 (2001).
[23] C. Thiel, T. Böttger, and R. Cone, J. Lumin. **131**, 353 (2011).
[24] C. W. Thiel *et al.*, J. Lumin. **130**, 1598 (2010).
[25] R. R. Reibel *et al.*, J. Lumin. **107**, 103 (2004).
[26] S. A. Moiseev and B. S. Ham, Phys. Rev. A **70**, 063809 (2004).
[27] H. de Riedmatten *et al.*, Nature (London) **456**, 773 (2008).
[28] M. Hosseini *et al.*, Nature (London) **461**, 241 (2009).
[29] S. A. Moiseev and W. Tittel, Phys. Rev. A **82**, 012309 (2010).
[30] S. Massar and S. Popescu, Phys. Rev. Lett. **74**, 1259 (1995).
[31] V. Bužek and M. Hillery, Phys. Rev. A **54**, 1844 (1996).
[32] W. Sohler *et al.*, Opt. Photonics News **19**, 24 (2008).